International Journal of Coal Geology 215 (2019) 103304

Contents lists available at ScienceDirect

International Journal of Coal Geology

journal homepage: www.elsevier.com/locate/coal

Marine derived $^{87}Sr/^{86}Sr$ in coal, a new key to geochronology and palaeoenvironment: Elucidation of the India-Eurasia and China-Indochina collisions in Yunnan, China

Baruch F. Spiro[a,b,1], Jingjing Liu[a,c,1], Shifeng Dai[a,d,1,*], Rongshu Zeng[e], David Large[f], David French[g]

[a] State Key Laboratory of Coal Resources and Safe Mining, China University of Mining and Technology, China
[b] Department of Earth Sciences, Natural History Museum, Cromwell Road, London SW7 5BD, UK
[c] School of Resources and Geosciences, China University of Mining and Technology, Xuzhou 221116, China
[d] College of Geoscience and Survey Engineering, China University of Mining and Technology, Beijing 100083, China
[e] Institute of Geology and Geophysics, Chinese Academy of Sciences, Beijing, China
[f] Department of Chemical and Environmental Engineering University of Nottingham, Nottingham Road, Nottingham, UK
[g] School of Biological, Earth and Environmental Sciences, University of New South Wales, Sydney, Australia

ARTICLE INFO

Keywords:
Coal
Strontium isotopes
Geochronology
Palaeoenvironment
Terrestrial-marine correlation
China-Indochina collision

ABSTRACT

Coal has formed in terrestrial and coastal-marine environments from sub-polar to equatorial regions since the Devonian. It contains detailed long-term records of contemporaneous environment, climate, and subsequent modifications. However, in general, direct chronological information in coal has been sparse. The coal investigated in the present study is from the Mile intermontane basin, Yunnan Province, China, north of an arm of the Mesozoic Tethys Ocean. The coal contains marine geochemical signatures and syngenetic gypsum, common in coastal-marine sediments. The gypsum contains marine-derived Sr and, hence, has geochronological potential. The $^{87}Sr/^{86}Sr$ record (0.708350-0.708591) in the Mile coal agrees with time-calibrated $^{87}Sr/^{86}Sr$ records of marine planktonic foraminifera obtained from core DSDP 588C, 22.25-18.27 Ma (Early Miocene). The peat of the Mile coal was deposited over 4.6 Ma., which possibly is the longest deposition of a coal bed in the world to have been found today, although this duration should include the period of non-peat deposition or erosion if present during the time of the 4.6-Ma.

During this period, the regional geological structures were determined by the India-Eurasia collision, which resulted in transform faults with extensive rift structures, including the Mile rhomb-shaped graben. This structural setting enabled the flow of seawater from the South China Sea to reach inland graben structures, including that of the Mile Basin, where peat was deposited. Subsequent deformation caused by the South China-Indochina collision changed the regional structural and geographical-hydrological patterns. This affected the hydrology of the Mile Basin and resulted in its uplift to its present-day elevation of 1350 m.

This study is, to our knowledge, the first to use the marine-derived $^{87}Sr/^{86}Sr$ indicator and chronometer in coal. At present, marine-influenced peats generated in coastal salt marshes extend from the Arctic Ocean (Alaska and Siberia) in the north, to Patagonia and New Zealand in the south, while mangrove forests abound in equatorial and low-latitude coastal areas. The $^{87}Sr/^{86}Sr$ record of marine-influenced coal in this study area, provides a key for the determination of age-duration-rate of geological processes in the inland basin, associated with the closure of the Tethys Ocean. Results indicate that this method has potential for providing a temporal framework for geological events and processes in other areas. These may be found near marine shore lines across the globe dating back to the Devonian. Moreover, the $^{87}Sr/^{86}Sr$ signal in marine-influenced coal can be used for correlation with the well-established $^{87}Sr/^{86}Sr$ chronology of marine planktonic foraminifera. In turn, the $^{87}Sr/^{86}Sr$ signal provides a basis for correlating terrestrial records of climate and environment contained in this type of coal and associated sediments, with those of marine sediments, such as those based on $\delta^{18}O$ in planktonic foraminifera.

* Corresponding author.
E-mail address: daishifeng@gmail.com (S. Dai).
[1] Co-first authors, contributed equally to this work.

https://doi.org/10.1016/j.coal.2019.103304
Received 19 July 2019; Received in revised form 10 October 2019; Accepted 11 October 2019
Available online 17 October 2019

1. Introduction

Coal seams present complex systems composed of biogenic and non-biogenic organic and inorganic components (Ward, 2002, 2016; Finkelman et al., 2019). These can contain long-term (< 0.1 My to several My) continuous and detailed geological records in their organic matter, minerals, elements, and isotopes (Ward, 2016). These records are of sufficient duration to span key events in Earth's history, and can provide detailed information on the flora, environment, climate, hydrology, and basin evolution during their deposition; thermal history during burial; and other post depositional effects. Coal seams may represent longer periods than common terrestrial clastic sediments, making them more comprehensive and detailed archives (Large et al., 2003). However, this potential cannot be fully realised without sound temporal information. The age of coal is currently derived from palynomorphs, stratigraphic context (Cirilli, 2010; Greb, 2013), and radiogenic isotope chronology, such as U-Pb zircon and $^{40}Ar/^{39}Ar$ sanidine in tonsteins (Lyons et al., 2006; Dai et al., 2017) and Re-Os isotopic data of marine incursions in coal (Tripathy et al., 2015). However, the absence of tonsteins in coal limits the employment of volcanic ash to provide age limits for coal beds. Palynology as a geochronologic tool generally lacks precision, and, in many cases, independent verification of assigned age (Geboy et al., 2015). Some limitations may affect the usefulness of Re–Os geochronometry for coal beds (Geboy et al., 2015; Goswami et al., 2018). For example, although not strictly for use in marine deposits (cf. Cumming et al., 2012), most freshwater systems do not provide initial reservoirs that are both homogenous with respect to Re and Os and large enough to provide detectable amounts of these very rare trace elements (Geboy et al., 2015).

Of great interest are coals associated with key features in Earth's history, such as the area of the present study which was affected by major collision events: first by that of India and Eurasia, which resulted in the closure of the Tethys Ocean (Tapponnier et al., 2001) and later by that of China and Indochina (Leloup et al., 1995). The present study concentrates on the gypsum identified in the coal. It occurs as idiomorphic crystals in voids such as plant cells, indicating a process of syngenetic formation, before compaction. This observation raised the possibility of investigating its $^{87}Sr/^{86}Sr$ record as a potential geochemical indicator, and of testing its applicability as a chronometer in this key area of South East Asia, and potentially its wider application.

So far, the use of $^{87}Sr/^{86}Sr$ as a chronometer of marine sediments was based on the extensive studies of marine calcareous sediments and their carbonate biogenic components, in particular, planktonic foraminifera (Hodell et al., 1991). The temporal $^{87}Sr/^{86}Sr$ record of seawater, as preserved in chemical and biogenic carbonates, has become a powerful tool for dating and correlating marine carbonates (e.g., Veizer and Compston, 1974.; Burke et al., 1982; Elderfield, 1986; Hodell et al., 1991; Veizer et al., 1997). Hodell et al. (1991) presented a very detailed high-resolution study of $^{87}Sr/^{86}Sr$ in planktonic foraminifera in Miocene sediments from cores DSDP 588A and DSDP 588C (Western Pacific Ocean east of Australia, 26°06.7′S and 161°13.6′E). The $^{87}Sr/^{86}Sr$ depth profile was calibrated on the basis of magneto-stratigraphy and oxygen isotope stratigraphy of the same core and can serve as a reference for the results of the present study. The relation plots of $^{87}Sr/^{86}Sr$ and age for DSDP 588C and DSDP 588A of Early and Middle Miocene ages, respectively (Hodell et al., 1991) are truly remarkable in their overall linear relationships for the Early and Middle Miocene, with considerable ranges of $^{87}Sr/^{86}Sr$ values.

The Mile M1 coal seam in the lower part of the Miocene Xiaolongtan Formation, is 27-m thick and is located at 1350-m elevation in the Mile intermontane basin in southern Yunnan, China (Fig. 1; Wang, 1995). The plan for the investigation of the $^{87}Sr/^{86}Sr$ record in the Mile coal was: first, to determine whether or not the coal was deposited in an environment affected by seawater, and whether the gypsum displays features indicative of syngenetic origin. If these criteria are met then to explore the use of the $^{87}Sr/^{86}Sr$ record of the gypsum as a chronometer for the environmental record contained in the coal, and, furthermore, to attempt to relate the $^{87}Sr/^{86}Sr$ record to the regional tectonic evolution. Such approach could then be attempted in the study of many coals

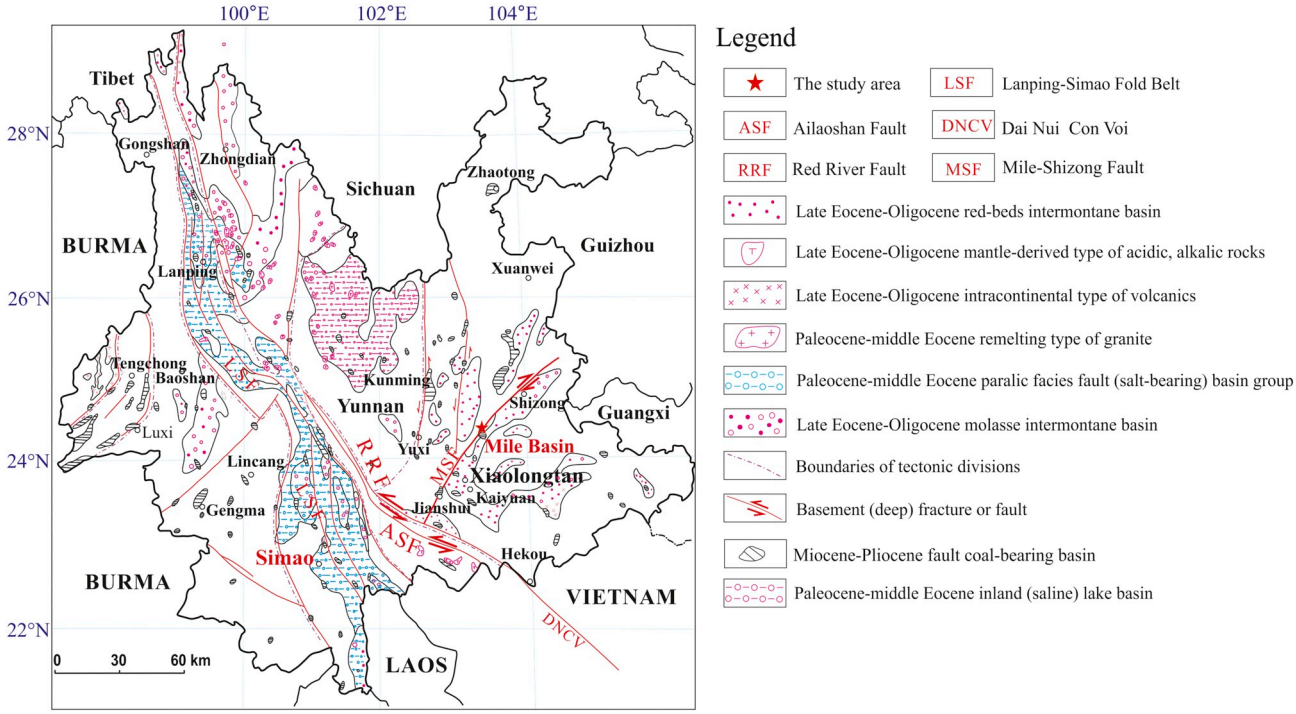

Fig. 1. Structural map of Yunnan Province, China, and its Palaeogene-Neogene sedimentary basins. The Mile basin is located on right lateral Mile-Shizong fault. It reaches the left lateral Red River Fault (RRF) and Ailao Shan Fault (ASF) which together form the Red River Ailao Shan Fault Zone (RRASFZ) (modified from Wang, 1995).

showing geochemical indications of syngenetic seawater effects (e.g., most coals with total S > 1%), which have wide temporal and geographical distributions (Chou, 2012), although caution should be considered because high sulfur in some coals can result from marine influence after burial and diagenesis or from hydrothermal solutions, which can happen in all stages of coal formation from peat accumulation through diagenetic to latter epigenetic processes. Therefore, it is crucial to identify whether or not the sulfur in coal was syngenetically derived from seawater during peat deposition. For example, in this study, no veins or other indicators for effects of post depositional fluids were observed, as described below.

2. Geological background

The Mile Basin is structurally connected via the ~50-km long Mile-Shizong Fault (MSF) to the Red River Fault (RRF)-Ailaoshan (ASF) Transform Fault Zone (RRASTFZ), which reaches the South China Sea (Fig. 1). The RRASTFZ resulted from the northward movement of Indochina, its collision with China, and the closure of the Tethys Ocean during the Cretaceous (Fig. 2A; Cai and Zhang, 2009; Leloup et al., 1995; Wang et al., 2000; Faure et al., 2014). The presence of seawater in this region is indicated by the $^{87}Sr/^{86}Sr$ values in salt deposits in the Simao Basin, south of the RRASTFZ (Figs. 1, 2A),ranging from 0.707121 (Jurassic seawater) to 0.709734 (Miocene seawater) (Zheng et al., 2012). This region had also been affected by continental fresh waters (Zheng et al., 2012). These features support the interpretation of uplift of the Simao Basin, which was initially at near sea level during the Miocene, with increasing contribution of surface water later (Zheng et al., 2012).

Furthermore, within the RRASTFZ, Palaeogene sediments contain gypsum and floral remains: the former indicates a similar environmental condition, and the latter belong to the same species as those of the Miocene Xiaolongtan Formation (Shoenbohm et al., 2005; Wang, 1995), indicating a similar ecology and habitat of these floral remains. These similarities indicate that there was a hydrological connection between the RRASTFZ and Mile Basin through the Xiaojiang Fault. This hydrological connection allowed sea water to reach the Mile Basin (Blue circle in Fig. 2B) where peat was deposited as part of the sedimentary sequence of the Xiaolongtan Formation (Fig. 2B).

The present-day MSF and the RRASTFZ (Fig. 1) are related to major transform faults that extend to Tibet (Fig. 2B; Tapponnier et al., 2001), the left-lateral Xianshuihe-Xiaojiang and right-lateral Jiali strike-slip faults, which resulted from the earlier (~50 Ma) collision between the Indian and the Eurasian plates (Tapponnier et al., 2001) (Fig. 2B). The RRASTFZ extends to the South China Sea with an overall length of more than 1000 km (Tapponnier et al., 1990; Faure et al., 2014). The RRASTFZ started in the Permian or Triassic (Cai and Zhang, 2009; Leloup et al., 1995), and was initially right-lateral (Fig. 2B, Tapponnier et al., 2001; Fig. 2C, Schoenbohm et al., 2006). The fault subsequently changed to left-lateral due to the Indochina-China collision; there are a range of ages reported for this change, i.e., later than 27.5 Ma (Wang et al., 2000), 21 Ma (Searle, 2006), 22-17 Ma (Leloup et al., 1995), and 17 Ma (Xu et al., 2012) (Fig. 1, Wang, 1995; Fig. 2A, Cai and Zhang, 2009).

During the Miocene, peat was deposited in the graben of the Mile Basin (Wang, 1995). At that time, the graben of the Mile Basin (Fig. 2C) was part of the Xianshuihe-Xiaojiang left lateral fault system, which reached the RRASTFZ (Fig. 2B, 2C) (Tapponnier et al., 2001; Schoenbohm et al., 2006). However, the current Mile-Shizong fault is right-lateral and extends further to the North-East (Fig. 1; Wang, 1995). Therefore, the Mile Basin could contain the sedimentary records for the periods preceding and following the change in the regional structural

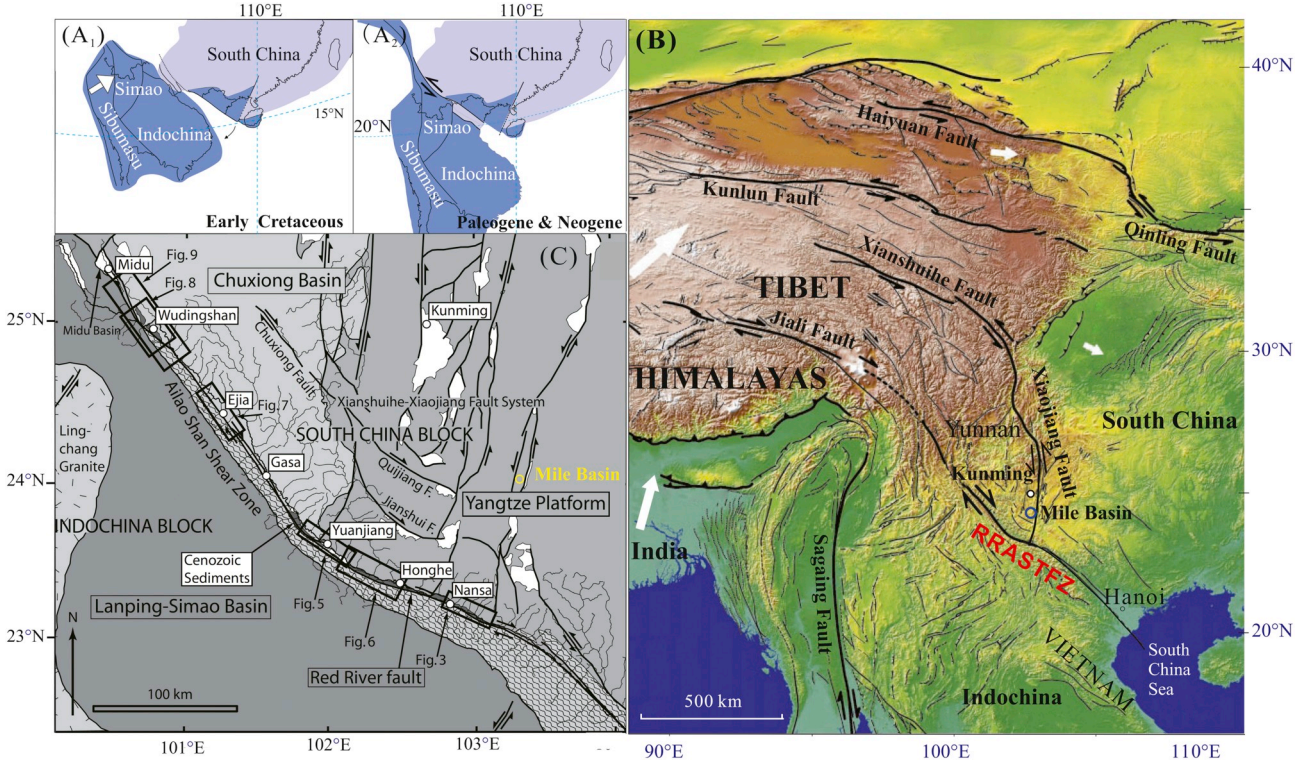

Fig. 2. Geological background of the Mile Basin. (A), Stages in the Indochina-South China collision which brought about the closure of the Palaeo-Tethys (modified from Cai and Zhang, 2009); A_1, Early Cretaceous, and A_2, Paleogene-Neogene. Note the overall change in geographical location and the relationship between China and Indochina. (B), Topography (present day) and principal faults in Tibet, Yunnan, and adjacent areas associated with earlier (~50 Ma) collision of the Indian and Eurasian plates and the uplift of Tibet (modified from Tapponnier et al., 2001). Note the right lateral RRASTFZ and the left lateral Xianshuihe fault, and the Xiaojiang Fault which contains the Mile Basin (Blue circle). (C), The NW-SE Red River Ailao Shan Fault Zone (RRASFZ) right lateral and the N-S Xianhuihe-Xiaojiang Fault Systen (left lateral), which includes the Mile Basin graben structure during Miocene times (modified from Schoenbohm et al., 2006).

patterns, as those originating from the India-Eurasia collision to those originating from the Indochina-China collision. The Mile coal serves as a long-term chronostratigraphic record of environmental, climatic, and hydrological features in relation to the reginal tectonic evolution, based on the coal characteristics and the geochemical compositions.

3. Samples and analytical methods

The coal mine of the M1 seam, Xialongtan Formation in the Mile Basin, is located near the Shanxin Village (103°23′06″ - 103°24′53″E and 24°13′06″ - 24°13′45″N), 142-km southeast of the province capital Kunming and 148-km south of the county capital Mengzi. The 27-m thick Mile (M1) coal seam is in the lower part of the 40-150-m thick Miocene Xiaolongtan Formation (Fig. 3), which is unconformably overlain by the Pliocene Shizongdu Formation. It uncomformably overlies the 150-530m thick siliciclastic Eocene-Oligocene Muhuaguo Formation, which in turn overlies the limestones of the Middle Triassic Gejiu Formation.

Bench samples (continuous sub-layers through the seam section) were taken from a vertical transect across the thickness of the Mile coal seam at the face of the mine. The total thickness of the coal seam in this section is 2700 cm. Each bench sample was between 6- and 50-cm thick, 10-cm wide, and 10-cm deep. Samples were immediately bagged in plastic to retain moisture and to diminish oxidation and contamination. Numbers and bench thicknesses of all samples are given in Table 1. From top to bottom, the 61 bench samples of coal are identified as ML-1 to ML-61. The seam includes two partings (18- and 10-cm thick; interbedded between the M-11 and M-13 and the M-46 and M-48 coal bench samples, respectively). Partings are referred to as non-coal sedimentary thin layers within the coal seam. The sample numbers of roof, parting, and floor samples (the top; intraseam non-coal layers; and the base) are identified with the suffixes R, P, and F, respectively.

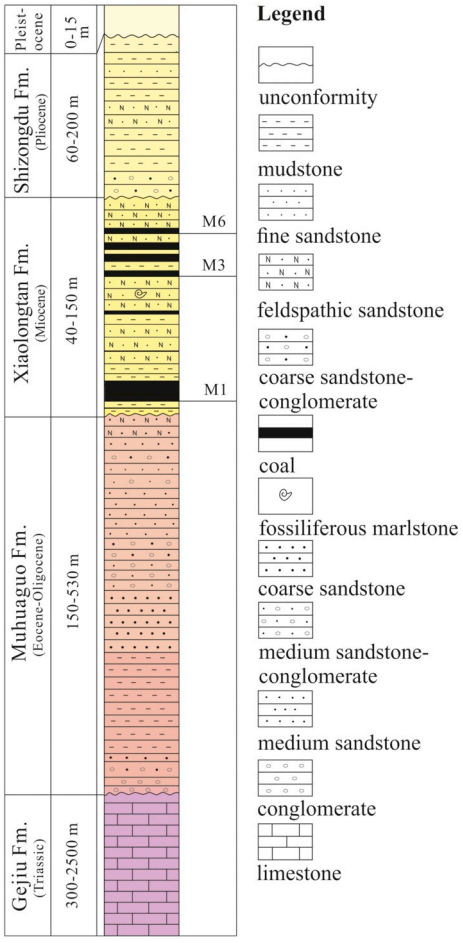

Fig. 3. Stratigraphic section in the Mile Basin. The M1 seam is located in the lowermost Miocene Xiaolongtan Fm. (modified from Wang, 1995).

Proximate analysis, which includes moisture content, ash yield, and volatile matter content, was performed following ASTM Standards D3173/D3173M-17a (2017), D3175-17 (2017), and D3174-12 (2012), respectively. The content of total sulfur ($S_{t,d}$) and those of the various forms of sulphur (sulphate sulphur, $S_{s,d}$; sulphide sulphur, $S_{p,d}$; and organic Sulphur, $S_{o,d}$) were determined following ASTM Standards D3177-02 (2011) and D2492-02 (2007), respectively. Based on ASTM standard D2798-11a (2011), huminite random reflectance (%R_o) was measured using a Leitz Orthoplan microscope with a 547 nm bandpass filter, 9-μm diameter measuring spot, and a photomultiplier calibrated using a series of glass reflectance standards in the range of coal reflectance values.

A scanning wave-length dispersive X-ray fluorescence spectrometer (XRF; Thermo ARL Advant'XP+) was used to determine the concentration of major element oxides (SiO_2, TiO_2, Al_2O_3, Fe_2O_3, MgO, CaO, MnO, Na_2O, K_2O, and P_2O_5) in high temperature ashes (815°C) of the samples. The concentrations of Sr and Ba were determined by inductively coupled plasma mass spectrometry (ICP-MS; ThermoFisher, X series II). ICP-MS analysis was carried out on samples prepared in the following procedure: 50-mg coal and non-coal rock samples were digested in a Milestone microwave digestion system (UltraClave Microwave High Pressure Reactor); coal samples were digested with 5-ml HNO_3 (65%) and 2-ml HF (40%); and non-coal samples were digested with 2-ml HNO_3 and 5-ml HF. Standard references (Inorganic Ventures CCS-4) were used for calibration of trace element concentrations.

A field emission-scanning electron microscope (FE-SEM, FEI Quanta™ 650 FEG), in conjunction with an energy-dispersive X-ray spectrometer (EDAX; Genesis Apex 4), was used to study the general features of the coal samples and features of the minerals and their chemical compositions in particular. Polished block samples were carbon-coated using a Quorum Q150T ES sputtering coater. The working distance of the FE-SEM was 10 mm, beam voltage 20.0 kV, aperture 6, and spot size 5. The images were captured via a retractable solid-state back scattered electron detector.

The mineralogical compositions were determined by X-ray powder diffraction after the coal samples were ashed at a low-temperature (< 120°C) using an EMITECH K1050X plasma asher. X-ray diffraction (XRD) analysis was performed on powdered sample aliquots after low-temperature ashing. Analysis was performed on a diffractometer (D/max-2500/PC XRD) with Ni-filtered Cu-Kα radiation and a scintillation detector. The XRD pattern was recorded over a 2θ interval of 2.6–70°, with a step size of 0.01°.

A total of 13 samples containing gypsum as detected by XRD were chosen for $^{87}Sr/^{86}Sr$ analyses, which were listed in Table 1. These coal samples for $^{87}Sr/^{86}Sr$ analyses have relatively higher Ca content (2.25-4.76%, 3.65% on average) but lower ash yields (6.12-22.19%, 12.55% on average), relative to those with non-detectable gypsum by XRD (Ca: 0.42-3.90%, 2.79% on average; ash yield: 3.6-50.1%, 15.06% on average). The preparation of samples for $^{87}Sr/^{86}Sr$ analyses is based on the methods described by Li et al. (2015). The first step of the procedure is as follows: an aliquot (~ 6 g) of each powdered (< 200 mesh) coal sample was loaded into a glass beaker, mixed with ultrapure water (300 ml, 18.2 MΩ cm), vigorously stirred and then left overnight to allow gypsum to completely dissolve (Li et al., 2015). The solution was prepared for $^{87}Sr/^{86}Sr$ determination by column separation (Li et al., 2015). The $^{87}Sr/^{86}Sr$ isotopic measurements were performed at the Institute of Geology and Geophysics CAS Beijing, on a Triton Plus TIMS using a double Re filament configuration. The Sr isotopic data were acquired in the static collection mode. Measured values were normalized for mass fractionation to $^{86}Sr/^{88}Sr = 0.1194$ (Li et al., 2015). NIST standard reference NBS-987 was used to evaluate instrument stability

Table 1
Sample number, depth (cm, from the top of coal seam), thickness (T, cm), proximate and sulfur analysis (%), huminite random reflectance (%R_o), elements, and $^{87}Sr/^{86}Sr$ in the Mile coals. M, moisture; A, ash yield; V, volatile matter; S_t, total sulfur; S_s, sulfate sulfur; S_p, pyrite sulfur; S_o, organic sulfur. ad, as-received basis; d, dry basis; daf, dry and ash-free basis. CaO and P_2O_5 are in wt. %; Sr and Ba are in ppm. MV, mean value based on the interval thickness of coal benches. The elemental concentrations are on a whole coal basis. Samples with $^{87}Sr/^{86}Sr$ values have detectable gypsum by XRD analysis.

Sample	Depth (cm)	T	M_{ad}	A_d	V_{daf}	$S_{t,d}$	$S_{s,d}$	$S_{p,d}$	$S_{o,d}$	R_o	CaO	P_2O_5	Sr	Ba	Sr/Ba	$^{87}Sr/^{86}Sr$
M-1-R	10	10		80.3							0.753	0.153	160.16	255.01	0.63	
M-2	30	20	9.84	50.1	67.18	0.61					1.641	0.119	173.45	218.62	0.79	
M-3	80	50	18.35	8.26	56.47	0.43					2.248	0.012	109.04	88.62	1.23	0.708573
M-4	130	50	18.48	11.62	55.88	0.85					2.875	0.033	151.24	137.34	1.10	
M-5	180	50	17.45	7.78	53.62	0.50				0.43	2.322	0.008	120.47	98.97	1.22	
M-6	197	17	18.58	11.5	54.24	1.26	0.33	0.07	0.86		3.286	0.015	153.96	130.57	1.18	
M-7	230	33	18.06	11.05	57.89	1.42	1.23	0.19	bdl		3.008	0.017	124.80	92.72	1.35	0.708591
M-8	280	50	17.35	9.83	57.48	0.84					2.641	0.040	139.12	114.80	1.21	
M-9	330	50	16.50	8.47	57.10	0.27					2.377	0.024	121.99	96.06	1.27	
M-10	385	55	15.65	15.11	57.38	0.75					2.409	0.030	131.74	112.67	1.17	
M-11	395	10		44.04							1.632	0.088	165.68	172.98	0.96	
M-12-P	413	18		70.65							1.006	0.129	175.96	230.03	0.76	
M-13	463	50	16.13	25.43	57.48	1.33	1.2	0.13	bdl		2.537	0.072	168.44	157.11	1.07	
M-14	513	50	16.73	16.2	58.76	1.25	0.52	0.09	0.64		2.978	0.116	248.95	182.81	1.36	
M-15	563	50	17.69	11.11	55.96	0.80					2.723	0.021	136.97	102.71	1.33	
M-16	591	28	16.80	16.25	58.73	0.95					3.393	0.058	204.86	171.79	1.19	0.708562
M-17	606	15	15.78	10.66	63.11	0.60					3.354	0.048	174.13	142.29	1.22	
M-18	636	30	16.31	8.62	58.95	0.40				0.38	2.783	0.023	131.91	96.77	1.36	
M-19	658	22	13.28	10.97	66.28	0.42					2.533	0.095	223.21	155.94	1.43	
M-20	708	50	14.99	7.68	58.40	0.24					2.668	0.019	137.95	102.25	1.35	
M-21	758	50	16.90	6.79	57.83	0.35					2.375	0.010	125.19	88.40	1.42	
M-22	808	50	18.56	10.48	56.32	0.46					3.249	0.013	186.39	147.90	1.26	
M-23	848	40	19.06	9.78	54.25	0.58					3.715	0.013	206.29	156.61	1.32	
M-24	854	6	13.39	14.65	66.21	0.68					3.040	0.019	160.07	137.53	1.16	
M-25	904	50	19.70	11.48	57.10	0.82					3.586	0.015	185.18	126.84	1.46	
M-26	954	50	18.77	9.45	42.48	0.40					2.963	0.018	156.68	105.14	1.49	
M-27	1004	50	15.91	8.23	58.92	0.32					2.708	0.060	198.01	118.74	1.67	
M-28	1054	50	16.57	7.59	58.84	0.05				0.32	2.646	0.066	209.71	120.31	1.74	
M-29	1104	50	15.86	7.29	59.80	0.19					2.627	0.016	145.68	94.98	1.53	0.708402
M-30	1154	50	16.70	6.73	57.58	0.23					2.476	0.010	135.29	79.49	1.70	
M-31	1204	50	16.80	6.68	56.79	0.30					2.419	0.019	140.72	81.21	1.73	
M-32	1244	40	11.67	3.6	63.71	0.27					1.231	0.005	61.73	33.37	1.85	
M-33	1294	50	16.01	6.66	58.97	0.26					2.508	0.005	140.09	82.42	1.70	
M-34	1344	50	16.08	6.12	56.16	0.28					2.722	0.004	152.43	88.60	1.72	0.708480
M-35	1394	50	17.82	10.13	55.72	0.77					3.654	0.012	199.36	123.63	1.61	
M-36	1396	2	10.04	19.2	69.07	0.79					2.889	0.364	645.46	299.82	2.15	
M-37	1481	85	16.39	11.73	57.96	0.79					3.631	0.105	357.44	181.65	1.97	
M-38	1542	61	16.03	11.25	58.51	0.87					3.573	0.223	485.66	233.82	2.08	0.708486
M-39	1546	4	12.06	14.54	67.26	0.63				0.40	3.219	0.589	1011.28	435.60	2.32	
M-40	1601	55	16.32	12.43	57.73	0.61					2.879	0.025	189.49	122.97	1.54	
M-41	1701	100	15.29	20.82	59.64	0.80					2.805	0.028	202.54	134.24	1.51	
M-42	1786	85	16.58	13.78	59.23	0.67					3.462	0.057	281.34	168.75	1.67	
M-43	1836	50	15.20	11.74	59.46	0.35					3.064	0.054	251.16	150.02	1.67	
M-44	1896	60	14.77	16.55	59.49	0.48					3.088	0.025	212.58	148.81	1.43	
M-45	1961	65	18.52	12.38	56.40	1.09	0.07	0.01	1.01		4.649	0.020	261.75	158.56	1.65	0.708445
M-46	2001	40	17.32	17.93	56.82	2.06	0.53	0.36	1.18		4.450	0.041	288.23	171.17	1.68	0.708358
M-47-P	2011	10		75.86							1.133	0.149	194.95	227.09	0.86	
M-48	2061	50	17.86	22.19	61.43	3.60	1.3	0.45	1.85		4.758	0.033	310.33	196.24	1.58	0.708350
M-49	2111	50	16.86	17.39	58.91	3.78	1.52	0.44	1.81	0.45	4.569	0.019	272.59	163.48	1.67	0.708418
M-50	2161	50	16.45	17.46	61.87	1.57	0.82	0.02	0.73		4.342	0.025	263.53	193.78	1.36	0.708402
M-51	2221	60	16.57	17	59.96	0.89					3.521	0.022	215.64	149.51	1.44	
M-52	2281	60	15.81	7.42	59.31	0.32					3.383	0.010	194.65	109.10	1.78	0.708380
M-53	2341	60	16.56	8.15	55.64	0.66					3.710	0.011	225.20	133.80	1.68	0.708433
M-54	2391	50	20.84	18.54	57.50	0.50					3.257	0.034	251.26	197.79	1.27	
M-55	2441	50	16.32	7.66	56.91	0.39					3.254	0.015	218.30	133.97	1.63	
M-56	2496	55	16.49	13.02	59.22	0.34					3.137	0.031	226.26	142.51	1.59	
M-57	2561	65	17.81	9.56	54.81	0.64					3.900	0.033	249.65	136.33	1.83	
M-58	2616	55	16.33	25.88	60.11	0.98					0.418	0.018	334.42	252.52	1.32	
M-59	2671	55	12.67	45.3	66.28	1.00					2.566	0.039	243.53	225.32	1.08	
M-60	2711	40	12.61	43.72	66.79	0.96					2.480	0.038	218.30	211.10	1.03	
M-61-F	2741	30		53.24							2.100	0.049	203.14	241.78	0.84	
MV			16.11	13.56	57.26	0.76				0.40	3.184	0.055	233.20	149.50	1.56	
Chou[a]						> 3										
Heshan[b]						2-8.5					2.9*	0.03*	704[b]	107[b]	6.58	
Guiding[c]						6.51					1.11	0.012	182	68	2.67	
Yanshan[d]						10.65					0.85	0.022	186.5	76	2.45	
UK[e]						2										
Variscan[f]						4.19										

bdl, below detection limit. *, on ash basis. a, marine-influenced coals around the world (Chou, 2012). b, marine-influenced coals in the Heshan Coalfield, Guangxi Province, China (Dai et al., 2013). c, marine-influenced coals in the Guiding Coalfield, Guizhou Province, China (Dai et al., 2015). d, marine-influenced coals in the Yanshan Coalfield, Yunnan Province, China (Dai et al., 2008). e, marine-influenced coals in the United Kingdom (Spears, 2017). f, marine-influenced coals from the South Wales Variscan foreland basin, UK (Gayer et al., 1999).

during the period of data collection. The measured average value of the NBS-987 was $^{87}Sr/^{86}Sr = 0.710240 \pm 0.000010$, in good agreement with the reported values (Li et al., 2015).

Technically, there are no uncertainties in age estimates associated with this technique because the Sr isotopic compositions were exclusively determined in the water-soluble gypsum in the coal. Any acids, for example, HCl, HF, and HNO3 which are generally used for coal sample digestion or leaching, were not used in this study, and hence no Sr derived from aluminosilicates from coal samples was leached. Therefore, it is not necessary to further calibrate the age derived from Sr isotopes in this study.

4. Results

4.1. Coal characteristics

The samples of floor, roof, and partings have high values of mineral content/ash yield (A_d), with $A_d > 50\%$, whilst the coal benches have low A_d values (3.6 to 40.0%, mean 13.6%; Table 1). The wide range of A_d values largely reflects the variations in the input of surficial mineral matter. The average values of huminite random reflectance (%R_o) and volatile matter (dry and ash free basis) are 0.40% and 57.3%, respectively (Table 1), indicating a subbituminous level of coalification.

The depth profiles of A_d and indicative elements of the coal seam show distinct patterns (Fig. 4). Within the coal benches, the distribution of CaO, $S_{t,d}$, P_2O_5, Sr, and Ba show two major sections bordered approximately at a depth of 1344 cm (red dash line in Fig. 4). The lower section has higher concentration of these elements than the upper section (Fig. 4). Both the upper and the lower sections contain a thin ash-rich layer (parting), one at ca. 400-cm and the other at 2000-cm depth. The two partings are marked by low values of CaO and $S_{t,d}$, low Sr/Ba ratios, similar to the ash-rich coal benches close to the floor and roof. A nearly pure coal ($A_d = 3.6\%$), occurs in the middle of the seam (sample M32; at a depth of 1204-1244 cm).

4.2. Indications for seawater effects

The content of $S_{t,d}$ ranges from 0.05 to 3.78% (Table 1) with a mean value of 0.76%. It is high in part of the lower section 2000-2100 cm (3.6-3.78%) but it is not higher than 1.57% elsewhere, with the exception of sample M42 with a total sulfur of 2.06% (Fig. 4). Overall, the high values of $S_{t,d}$ coincide with high values of Ca, Sr, and Ba. Considerable parts of the section have $S_{t,d}$ values > 1% (Table 1; also the vertical black dash line in Fig. 4), and the organic and sulphate sulphur contents account for ~50% and ~40% of $S_{t,d}$, respectively, indicating seawater influence, as suggested by Chou (2012) for coals in other areas.

The distribution of P_2O_5 shows the high values at 1394-1546 cm and 385-513 cm depth, coinciding with high concentrations of Ca, Sr, and Ba (Fig. 4), which may be related to particularly strong effect of seawater (Morris et al., 1981).

The sea water related minerals in this study, i.e., gypsum ($CaSO_4.2H_2O$) and the crandalite-goyazite-gorceixite series (Ca- Sr,- Ba-) aluminophosphate hydrates, were identified as void fillings (Fig. 5C).

The global average concentrations of Sr and Ba in modern oceans are 8.0 and 0.013 mg/l and in stream waters 0.07 and 0.02 mg/l, respectively (Reimann and de Caritat, 1998). The concentrations of Sr and Ba and their ratio may be used as indicators for ambient water, in terms of seawater and freshwater and their mixtures (Schmitz et al., 1991; Arai and Hirata, 2006). The Sr/Ba ratio could, therefore, indicate a seawater/freshwater effect in coal. The profile of Sr/Ba in the Mile coal (Fig. 4) shows high values in the coal benches, and low values in floor, roof, partings, and coal benches that are in direct contact with them and have slightly higher A_d values.

This distinction is further illustrated in the Sr/Ba vs. A_d plot (Fig. 6). The samples with low-A_d (< 40%, mostly < 22%) have Sr/Ba values > 1.0, whilst those with high-A_d (44-80%) have Sr/Ba values < 1.0, and show a general negative correlation between Sr/Ba and A_d. The boundary at Sr/Ba = 1.0 provides a criterion for interpreting the Sr/Ba depth profile as a marine/freshwater indicator (Fig. 6). Hence, coal

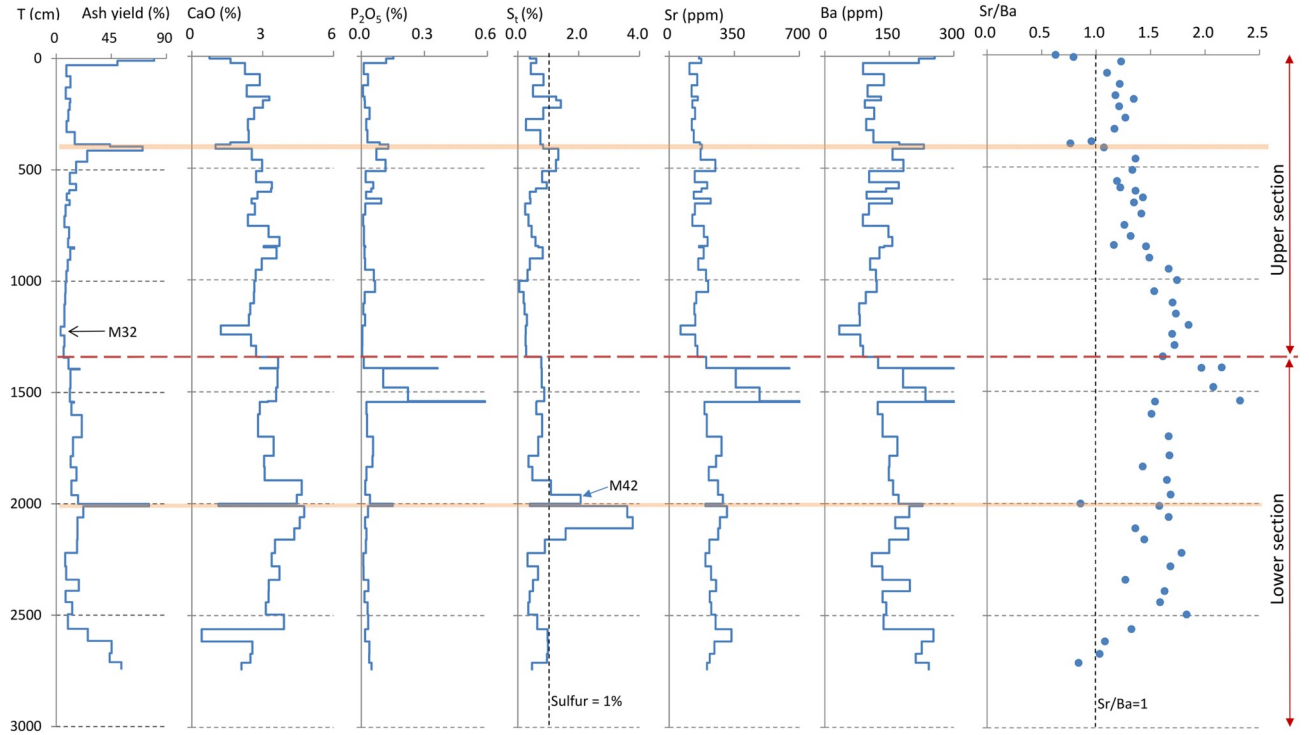

Fig. 4. Depth profiles of ash yield (A_d), CaO, P_2O_5, $S_{t,d}$ (total sulphur) Sr, Ba, and Sr/Ba through the Mile M1 coal seam. The horizonal yellow strips marked in the figure show the partings within the coal seam. Depth in cm.

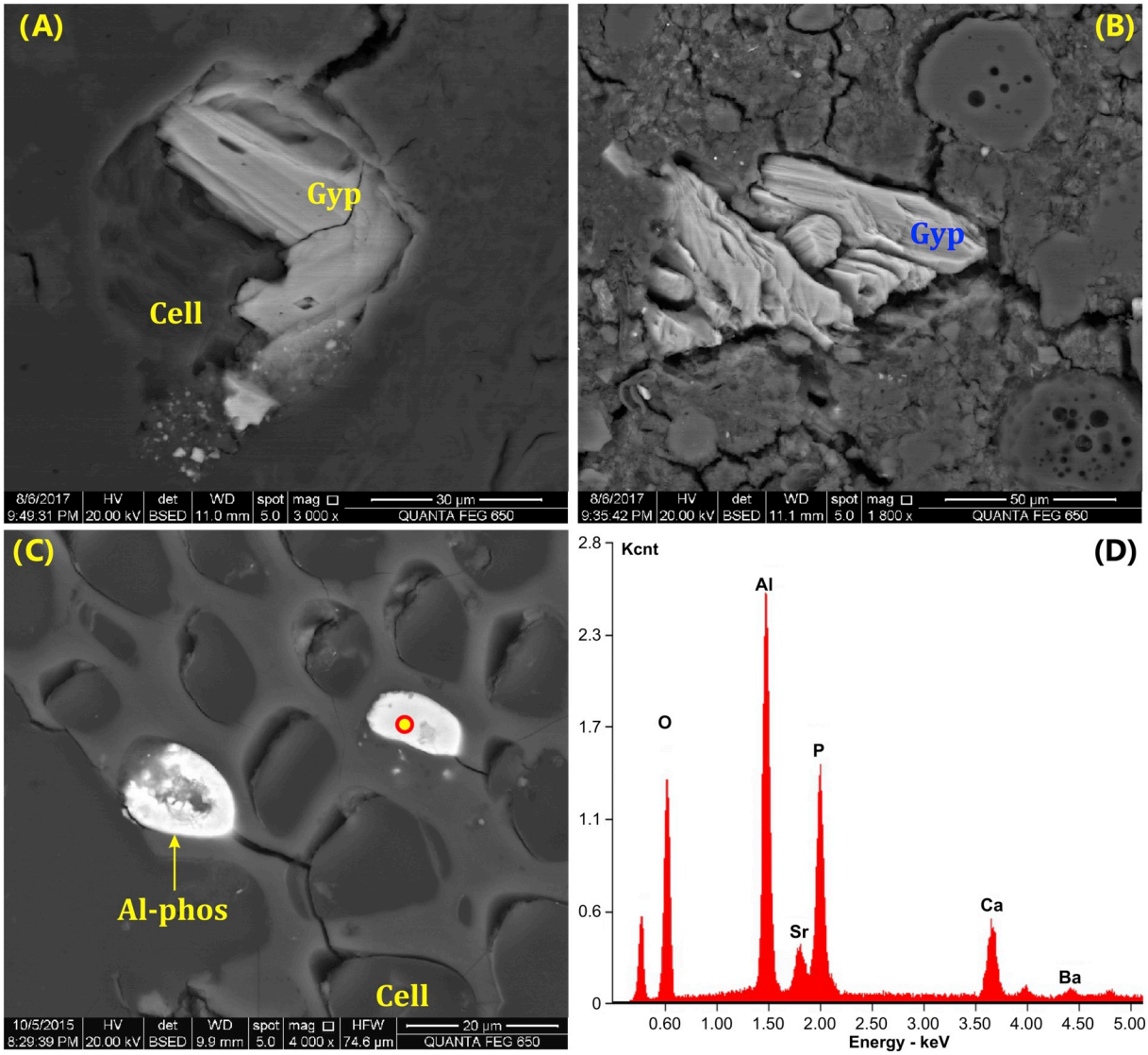

Fig. 5. Syngenetic minerals in the Mile coal: (A) and (B), gypsum filling plant cells and cavities in the organic matter. (C), Ca-, Sr-, and Ba-aluminophosphates (representing members of the crandalite-goyazite-gorceizite group) as plant-cell fillings. (A)-(C), SEM backscattered electron images. (D), Energy Dispersive X-Ray Spectrum of the test spot in (C). Gyp, gypsum; cell, coal-forming plant cell; Al-phos, Ca-, Sr-, and Ba-aluminophosphates.

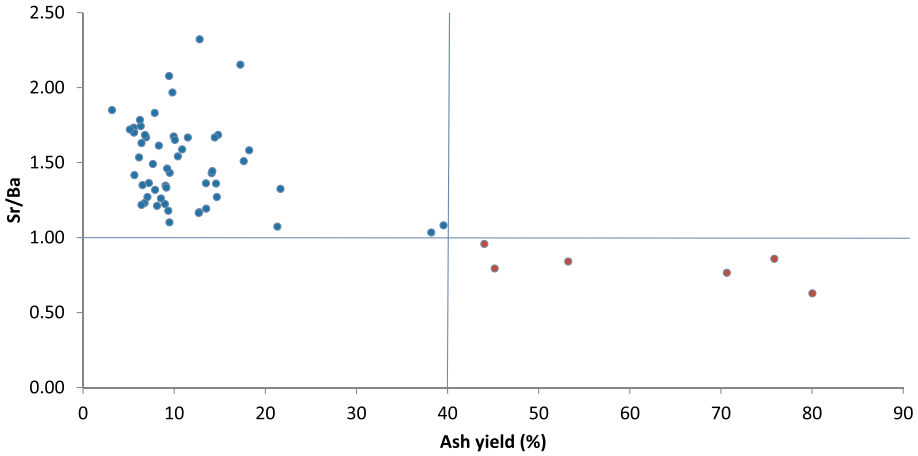

Fig. 6. Diagram of ash yield (A_d, %) and Sr/Ba. Coal samples with A_d < 40% (mostly < 20%; blue circles in the figure) and Sr/Ba > 1.0 have been subjected to the influence of sea water. Floor, roof, partings, and high-ash coal (red circles in the figure), all with A_d > 40% and Sr/Ba < 1.0, have been subjected to the influence of fresh water.

with gypsum (A_d < 40%, Sr/Ba > 1) shows the influence of seawater, while floor, roof, and partings (A_d > 40%, Sr/Ba < 1) seem to be associated with freshwater. The concentration of Sr in seawater is > 100 times higher than in river water (Reimann and de Caritat, 1998); therefore, a minor seawater contribution to a freshwater reservoir would dominate the $^{87}Sr/^{86}Sr$ values of the mixture.

The overarching trend of Sr/Ba and CaO in the coal benches with stratigraphy (Fig. 4) is a steep increase followed by a gradual decrease, reflecting variations in the relative contribution of seawater and freshwater. This long term trend is punctuated by episodes of strong freshwater influence as indicated by Sr/Ba < 1, occurring in layers rich in terrigenous mineral matter, i.e., the partings. These episodes of fresh water influx may primarily reflect a wet climate.

4.3. Gypsum in the coal and its $^{87}Sr/^{86}Sr$ values

Gypsum was identified by XRD in many coal benches of the seam. Under the SEM-EDS, gypsum showed typical plate-like crystals in plant cells or small vugs (Fig. 5A,B). These textures are indicative of syngenetic formation (Ward, 2002, 2016), i.e. derived from the original pore water before compaction. Gypsum may contain Sr and its $^{87}Sr/^{86}Sr$ values would indicate the signature of the parent solution. The plot of the $^{87}Sr/^{86}Sr$ values and the ash yields (A_d) (Fig. 7) does not show a distinct relationship between them. As the high A_d values may reflect episodes of enhanced deposition of detrital terrigenous mineral matter likely transported by freshwater during peatformation, the $^{87}Sr/^{86}Sr$ results perhaps do not show effects of the source of terrigenous mineral matter but may reflect primarily the seawater effects.

4.4. Temporal interpretation of $^{87}Sr/^{86}Sr$ record in the Mile coal

The $^{87}Sr/^{86}Sr$ record of gypsum in the Mile coal was interpreted with reference to the $^{87}Sr/^{86}Sr$ and age of planktonic foraminifera obtained from core DSDP 588C (Hodell et al., 1991). The chronology of these oceanic sediments was based on magneto-stratigraphy and oxygen isotope stratigraphy (Hodell et al., 1991) as presented in Fig. 8A. The analytical precision for the $^{87}Sr/^{86}Sr$ results ($\pm 1.0 \times 10^{-5}$, 2 sigma) in the present study is the same as that of Hodell et al. (1991).

The $^{87}Sr/^{86}Sr$ values of gypsum (water soluble), along the depth profile of the coal (Table 1) range between 0.708350 (sample M48) and 0.708591 (sample M7) (Fig. 8B). The section of the record by Hodell et al. (1991) relevant to that of the Mile coal seam is given in Fig. 8C. The $^{87}Sr/^{86}Sr$ range from the Mile coal corresponds to the time span between 22.25 and 18.27 Ma, an overall span of ca. 4.0 Ma in the Early Miocene. The uppermost and lowermost samples M3 and M53 in the coal seam section are ca. 30 cm below the roof and ca. 370 cm above the floor, respectively, and therefore, ca. 400 cm of coal are unaccounted for by the $^{87}Sr/^{86}Sr$ record. If these coal intervals are added, assuming a similar rate of deposition, the total time span for the peat deposition of the Mile coal seam would be ca. 4.6 Ma., which should include the period of non-peat deposition or erosion if present during that time. On the other hand, this coal seam is not a sequence of distinct coal beds that are now correlated as a single bed, because the same coal seam is distributed in a wider area.

Therefore, for the 27-m thick coal seam, 1 cm of coal may represent ca. 1700 years. The estimated compaction associated with the increase in coalification from peat to soft brown coal (R_o = 0.4%; Table 1) is ~2:1 (Stach et al., 1982). On this basis, 1 cm of the original peat may represent ca. 850 years and the rate of accumulation may be about 0.012 mm/year. The topic of duration of coal has been addressed by several approaches (Large and Marshall, 2014). The present new geochronological results may be a contribution to the deciphering the timing of events and rates of the processes.

During peat deposition, the Mile Basin was subsiding, but subsequently, the average rate of uplift from sea level at 18.27 Ma to 1350 m at present, is on average ca. 0.074 mm/year. This process may be similar to that of the older marine evaporitic Simao Basin located to the Southeast of the Mile Basin (Fig. 1), the latter of which was increasingly affected by surface water under a compressive tectonic regime (Zheng et al., 2012).

5. Discussion

5.1. Geotectonic significance of the seawater-derived $^{87}Sr/^{86}Sr$ in the Mile coal

The stratigraphic distribution of A_d and indicative elements in the M1 coal (Fig. 4) shows variation in the influence of seawater and meteoric water, both controlled by climate and perhaps tectonism, within the temporal framework recorded by the marine $^{87}Sr/^{86}Sr$ signal. The location of the Mile Basin at more than 50-km to the north of the RRASTFZ (Fig. 2B) renders sea-spray or tidal incursions to be unlikely sources of gypsum with marine $^{87}Sr/^{86}Sr$ signature.

A likely hydrological connection between the inland Mile Basin and the remnants of the Tethys Ocean in the RRASTFZ is a transform fault, part of the left-lateral Xianshuihe-Xiaojiang fault system (Tapponier et al., 1990; Schoenbohm et al., 2006), forerunner of the current Mile-Shizong Fault (Fig. 1), as discussed above. The closure of this arm of the Tethys Ocean was due to the China-Indochina collision with the left-lateral displacement on the RRASTFZ. This collision brought about compression deformation on a regional scale: the change from left- to right-lateral displacement on the Mile-Shizong fault (Figs. 2B, C, and

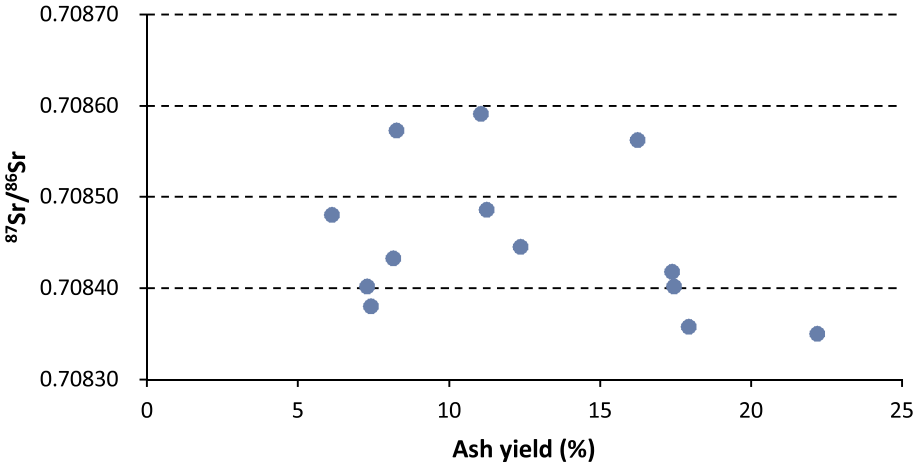

Fig. 7. Diagram of ash yield (%) and $^{87}Sr/^{86}Sr$ values in the Mile coal seam, suggesting that there is no relation between these parameters.

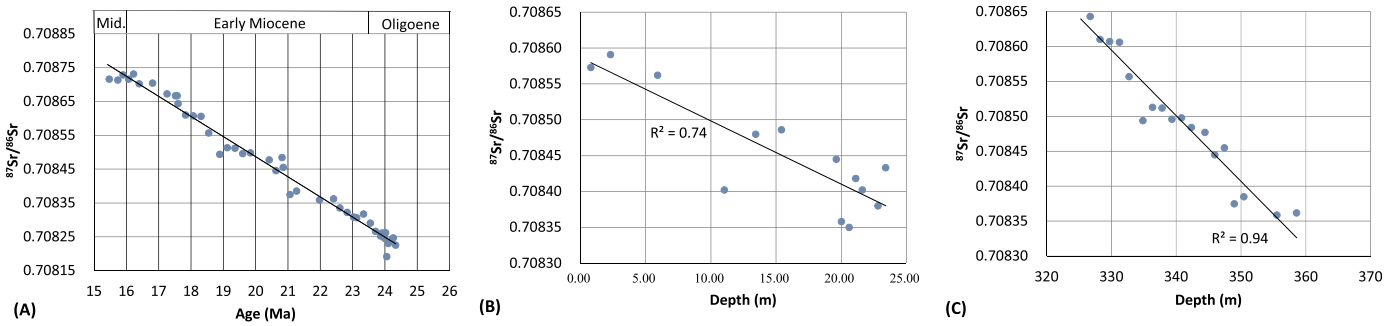

Fig. 8. The $^{87}Sr/^{86}Sr$ record of the Mile coal and in contemporaneous deep-sea sediments. (A), $^{87}Sr/^{86}Sr$ values of planktonic foraminifera of Early Miocene age (from DSDP 588C; Fig. 3 in Hodell et al., 1991). Mid., Middle Miocene. (B), $^{7}Sr/^{86}Sr$ values of gypsum in Mile coal seam. (C), the $^{87}Sr/^{86}Sr$ record in planktonic foraminifera in the same compositional range as in the Mile coal (Part of Fig. 8B).

1A, respectively) and the uplift of the area to the north of the RRASTFZ (Tapponnier et al., 1990; Schoenbohm et al., 2006). The new structural setting of the Mile Basin related to the China-Indochina collision caused the gradual decrease in the effect of seawater on the sedimentological and geochemical features of the M1 peat.

The record of variations in the concentrations of CaO, P_2O_5, S_{td}, Sr, Ba, and the Sr/Ba ratio, which are the result of variations in the contribution of seawater-derived solutes, and also of the occurrences of floor, roof, and partings composed of mineral-rich terrigenous sediments, is placed and assessed in a chronological framework.

The seawater $^{87}Sr/^{86}Sr$-based age span of the Mile coal (22.25-18.27 Ma) is within the range of the previously-suggested closure time of the Tethys Ocean in the RRASTFZ, the China-Indochina collision zone (Leloup et al., 1995). As discussed above, this fault zone was initially right lateral as a result of the India-Eurasia collision but changed to left lateral as a result of the China-Indochina collision (Fig. $2B_2$) (Leloup et al., 1995). This geotectonic change was studied extensively using radiogenic isotope geochronology, which generated a range of dates: later than 27.5 Ma (Wang et al., 2000) and 22-17 Ma (Leloup et al., 1995), and younger than 21 Ma (Searle, 2006) and 17 Ma (Xu et al., 2012). The agreement between the seawater $^{87}Sr/^{86}Sr$ based age span of the Mile coal (22.25-18.27 Ma) and the radiogenic isotope chronology derived from various petrologic phenomena related to tectonic activity along the RRASTFZ, part of the Jiali fault, indicates that the marine derived $^{87}Sr/^{86}Sr$ values in the Mile coal record the period when the Mile Basin was still controlled by, or under the influence of the left-lateral Xianshuihe-Xiaojiang fault system.

5.2. Significance of seawater derived $^{87}Sr/^{86}Sr$

The seawater-derived coal-based $^{87}Sr/^{86}Sr$ chronological framework of the Mile coal provides a new tool for the temporal interpretation of sedimentological, environmental, climatic and, potentially, biological information. This information has previously been based on several indicators such as geochemistry (Chou, 2012; Hentschel et al., 2016), mineralogy (Ward, 2002, 2016; Finkelman et al., 2019), and palynology (Jasper et al., 2010; Opluštil and Sýkorová, 2018).

The coal investigated was formed in a graben structure in a key area for the understanding of the evolution of SE Asia, which was controlled by two major tectonic processes: first the India-Eurasia collision and later the China-Indochina collision. A similar setting of a fault controlled inland basin is the Dead Sea Basin, part of the Syrian African Rift. During the Pliocene, it was fed by the Mediterranean Sea, part of the western Tethys via the ca. 50-km long fault-controlled Emek Ysreel valley, which leads to the Jordan Valley and the Dead Sea in the Syrian-African Rift (Zak, 1997; Stein et al., 2000; Katz and Starinsky, 2009). The $^{87}Sr/^{86}Sr$ record of the evaporitic Dead Sea sediments consisting of dolomite (0.7082-0.7083) and halite (0.7083-0.7087) differ from the Pliocene seawater source ($^{87}Sr/^{86}Sr \approx 0.7090$; Stein et al., 2000). The discrepancy was attributed to interaction between the Pliocene seawater and Cretaceous calcareous wall rocks of the Dead Sea Basin ($^{87}Sr/^{86}Sr \approx 0.7077$), which caused the dolomitisation and Sr isotope exchange (Stein et al., 2000).

The evaluation of the $^{87}Sr/^{86}Sr$ marine signal in coal requires the consideration of the mineralogical (gypsum) and chemical (Sr/Ba) characteristics indicative of seawater source. However, it is also necessary to take into account the lithology and geochemistry of the host rocks, which may have come into contact with the seawater that reached the coal. The contact may have been, for example, with the host rock within the depositional basin or with the host rocks of the RRASTFZ structurally-controlled seawater conduit. The interaction could take place near the seawater source, such as during tidal ingression, or at a distance from the sea along the conduit. In the case of the Mile Basin, the host rocks are pure siliciclastics (e.g., mudstone, sandstone with various grain sizes; Fig. 3). Furthermore, the very good agreement between the chronological indicators discussed above and this new $^{87}Sr/^{86}Sr$-based chronology confirms the absence of an effect of the limestones of the Triassic Gejiu Formation which underlies the Mile coal and is separated from the coal by the 150-530-m of the siliciclastic sediments of the Muhuaguo Fm. (Fig. 3).

The occurrence of coals and other organic-rich sediments associated with seawater depends primarily on the parent flora. Extensive halophyte flora occurs widely in salt marshes (> 0.5% NaCl) in coastal areas or around inland salt lakes. Coastal marine salt marshes extend from high latitude coastal areas in Alaska and Siberia in the north to Patagonia and New Zealand in the south, through mid-latitude temperate zones, to wide areas of extensive growth in the tropics (Fig. 9; Chapman, 1977).

Mangrove swamps are common in tropical seashore areas with species richness increasing from low values of five species at 30° North/South to > 50 near the equator (Ellison, 2002). Forested wetlands in freshwater were compared with those of salt-water environments, revealing significant differences (Lugo et al., 1988). Major characteristics, including net primary productivity, litter fall, and export of organic matter, are higher in salt-water forested wetlands than in freshwater ones (Lugo et al., 1988). Moreover, nutrient use efficiency by litter fall and litter turnover are higher in tidal salt-water wetlands than in freshwater wetlands (Lugo et al., 1988), indicating that they should be abundant.

These features indicate that coal and other organic-rich sediments deposited under the influence of seawater are probably common in the geological record. These have the potential of hosting and providing the seawater-derived gypsum which should contain the $^{87}Sr/^{86}Sr$ record of the contemporaneous seawater.

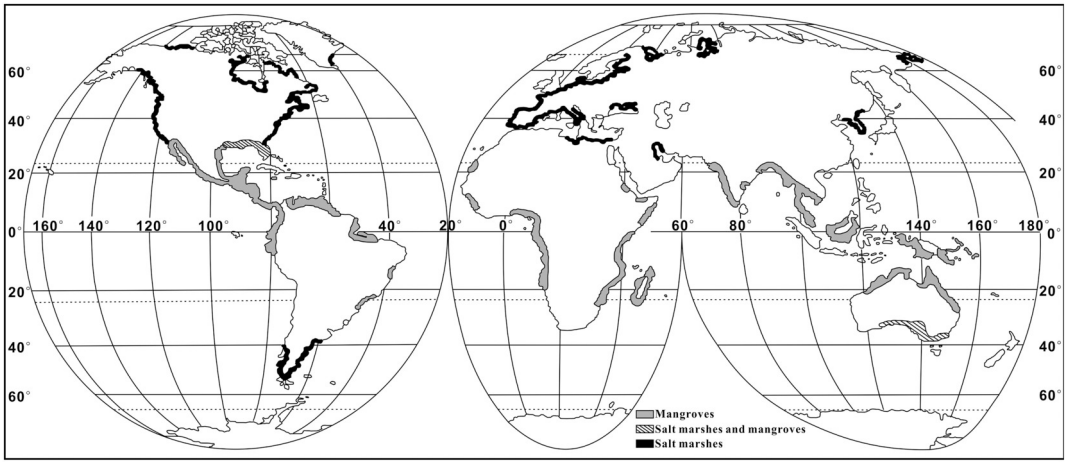

Fig. 9. Global distribution of salt marshes and mangrove swamps in coastal areas that support halophytes (Chapman, 1977). This wide distribution indicates the potential of the seawater- derived $^{87}Sr/^{86}Sr$ values in gypsum in peat and coal as a useful chronometer.

6. Summary

The investigation of gypsum and its water-soluble strontium in the Mile coal revealed that:

1) Gypsum in the coal occurs in platy crystals as fillings in plant cells and vugs, indicating a syngenetic origin, i.e. before compaction.
2) The $^{87}Sr/^{86}Sr$ values of the gypsum increases systematically from the base-floor to the roof of the Mile coal from 0.708350 to 0.708591, which corresponds to an age range of 22.25-18.27 Ma (Early Miocene) based on DSDP data. This is the first age of Sr isotopes derived from marine-influenced gypsum in coal. The peat of the Mile coal was deposited over 4.6 Ma., which possibly is the longest deposition of a coal bed in the world that have been found today, although this duration should include the period of non-peat deposition or erosion if present during the time of 4.6-Ma.
3) This age corresponds to radiometric ages determined in rocks in the Red River-Ailaoshan Transform Fault Zone, a major rift structure which extends to the South China Sea. This tectonic regime was associated with the India-Eurasia collision. The Mile Basin, a rhomb-shaped graben within the left-lateral Xiaojiang fault, was influenced by seawater. The subsequent Indochina-China collision changed the structural setting, ending the connection between the Mile Basin and the South China Sea.

The seawater-based $^{87}Sr/^{86}Sr$ chronology of the Mile coal can serve as a basis for the temporal interpretation of botanical, environmental, and climatic information in the study area. On a wider scale, the identification of marine-derived syngenetic gypsum in coal may lead to the establishment of a detailed and long-term chronology for near-shore terrestrial environments for the time span since the Devonian. Flora of salt marshes occurs currently from the Arctic to Patagonia, and Mangrove forests thrive in equatorial and low-latitude shores, suggesting potential for finding fossil equivalents close to marine shore lines across the globe, dating back to Devonian times. Moreover, the $^{87}Sr/^{86}Sr$ signal in marine-influenced coal can be used for correlation using the $^{87}Sr/^{86}Sr$ chronology of marine planktonic foraminifera. In turn, the $^{87}Sr/^{86}Sr$ signal provides a basis for investigating and correlating terrestrial records of climate and environment contained in this type of coal with those of marine sediments, such as the ones based on $\delta^{18}O$ in planktonic foraminifera and other calcareous taxa.

Declaration of Competing Interest

The authors declare that there is no conflict of Interest.

Acknowledgements

This work was supported by the National Natural Science Foundation of China (41420104001 and 41902164), the “111” Project (B17042), and the Program for Changjiang Scholars and Innovative Research Team in University (No. IRT_17R104).

References

Arai, T., Hirata, T., 2006. Differences in the trace element deposition in otoliths between marine- and freshwater-resident Japanese eels, *Anguilla japonica*, as determined by laser ablation ICPMS. Environ. Biol. Fish 75, 173–182.
Burke, W.H., Denison, R.E., Hetherington, E.A., Koepnick, R.B., Nelson, H.F., Otto, J.B., 1982. Variation of seawater $^{87}Sr/^{86}Sr$ throughout Phanerozoic time. Geology 10, 516–519.
Cai, J., Zhang, K., 2009. A new model for the Indochina and South China collision during the Late Permian to the Middle Triassic. Tectonophysics 467, 35–43.
Chapman, V.J. (Ed.), 1977. Wet coastal ecosystems. Elsevier, Amsterdam and New York (428 p).
Chou, C.-L., 2012. Sulfur in coals: a review of geochemistry and origins. Int. J. Coal Geol. 100, 1–13.
Cirilli, S., 2010. Upper Triassic–lowermost Jurassic palynology and palynostratigra-phy: a review. In: Lucas, S.G. (Ed.), The Triassic Timescale. Geol. Soc. (Lond.) Spec. Publ. 334. pp. 285–314.
Cumming, V.M., Selby, D., Lillis, P.G., 2012. Re-Os geochronology of the lacustrine Green River Formation: insights into direct depositional dating of lacustrine successions, Re-Os systematics and paleocontinental weathering. Earth Planet. Sci. Lett. 359, 194–205.
Dai, S., Ren, D., Zhou, Y., Chou, C.-L., Wang, X., Zhao, L., Zhu, X., 2008. Mineralogy and geochemistry of a superhigh-organic-sulfur coal, Yanshan Coalfield, Yunnan, China: evidence for a volcanic ash component and influence by submarine exhalation. Chem. Geol. 255, 182–194.
Dai, S., Zhang, W., Seredin, V.V., Ward, C.R., Hower, J.C., Song, W., Wang, X., Li, X., Zhao, L., Kang, H., Zheng, L., Wang, P., Zhou, D., 2013. Factors controlling geochemical and mineralogical compositions of coals preserved within marine carbonate successions: a case study from the Heshan Coalfield, southern China. Int. J. Coal Geol. 109–110, 77–100.
Dai, S., Seredin, V.V., Ward, C.R., Hower, J.C., Xing, Y., Zhang, W., Song, W., Wang, P., 2015. Enrichment of U–Se–Mo–Re–V in coals preserved within marine carbonate successions: geochemical and mineralogical data from the Late Permian Guiding Coalfield, Guizhou, China. Mineral. Deposita 50, 159–186.
Dai, S., Ward, C.R., Graham, I.T., French, D., Hower, J.C., Zhao, L., Wang, X., 2017. Altered volcanic ashes in coal and coal-bearing sequences: A review of their nature and significance. Earth-Sci. Rev. 175, 44–74.
Elderfield, H., 1986. Strontium isotope stratigraphy. Palaeogeogr. Palaeoclimatol. Palaeoecol. 57, 71–90.
Ellison, A.M., 2002. Macroecology of mangroves: large scale patterns and processes in tropical coastal forests. Trees 16, 181–194.
Faure, M., Leprevier, C., Van Nguyen, V., Van-Vu, T., Lin, W., Chen, Z., 2014. The South China block-Indochina collision: where, when, and how? J. Asian Earth Sci. 79, 260–274.
Finkelman, R.B., Dai, S., French, D., 2019. The importance of minerals in coal as the hosts of chemical elements. Int. J. Coal Geol. 212, 103251.
Gayer, R.A., Rose, M., Dehmer, J., Shao, L., 1999. Impact of sulphur and trace element geochemistry on the utilization of a marine-influenced coal—case study from the

South Wales Variscan foreland basin. Int. J. Coal Geol. 40, 151–174.
Geboy, N.J., Tripathy, G.R., Ruppert, L.F., Eble, C.F., Blake, B.M., Hannah, J.L., Stein, H.J., 2015. Re–Os age for the Lower–Middle Pennsylvanian Boundary and comparison with associated palynoflora. Int. J. Coal Geol. 140, 23–30.
Goswami, V., Hannah, J.L., Stein, H.J., 2018. Why terrestrial coals cannot be dated using the Re-Os geochronometer: Evidence from the Finnmark Platform, southern Barents Sea and the Fire Clay coal horizon, Central Appalachian Basin. Int. J. Coal Geol. 188, 121–135.
Greb, S.F., 2013. Coal more than a resource: Critical data for understanding a variety of earth-science concepts. Int. J. Coal Geol. 118, 15–32.
Hentschel, A., Esterle, J.S., Golding, S.D., Pacey, D.V., 2016. Petrologic and stable isotopic study of the Walloon Coal Measures, Surat Basin, Queensland: peat accumulation under changing climate and base level. Int. J. Coal Geol. 160-161, 11–27.
Hodell, D.A., Mueller, P.A., Garrido, J.R., 1991. Variations in the strontium isotopic composition of seawater during the Neogene. Geology 19, 24–27.
Jasper, K., Hartkopf-Fröder, C., Flajs, G., Littke, R., 2010. Evolution of Pennsylvanian (Late Carboniferous) peat swamps of the Ruhr Basin, Germany: Comparison of palynological, coal petrographical and organic geochemical data. Int. J. Coal Geol. 83, 346–365.
Katz, A., Starinsky, A., 2009. Geochemical history of the Dead Sea. Aquat. Geochem. 15, 159–194.
Large, D.J., Marshall, C., 2014. Use of carbon accumulation rates to estimate the duration of coal seams and the influence of atmospheric dust deposition on coal composition. Geol. Soc. Lond., Spec. Publ. 404, 303–315.
Large, D.J., Jones, T.F., Somerfield, C., Gorringe, M.C., Spiro, B., Macquaker, J.H.S., Atkin, B.P., 2003. A high-resolution terrestrial record of orbital climate forcing in coal. Geology 31, 303–306.
Leloup, P.H., Lacassin, R., Tapponnier, P., Schärer, U., Zhong, D., Liu, X., Zhang, L., Ji, S., Trinh, P.T., 1995. The Ailao Shan-Red River shear zone (Yunnan, China), Tertiary transform boundary of Indochina. Tectonophysics 251, 13–84.
Li, C., Guo, J., Chu, Z., Feng, L., Wang, X., 2015. Direct high-precision measurements of the $^{87}Sr/^{86}Sr$ isotope ratio in natural water without chemical separation using thermal ionization mass spectrometry equipped with 1012 Ω resistors. Anal. Chem. 87, 7426–7432.
Lugo, A.E., Brown, S., Brinson, M.M., 1988. Forested wetlands in freshwater and salt-water environments. Limnol. Oceanogr. 33, 894–909.
Lyons, P., Krogh, T., Kwok, Y., Davis, D., 2006. Radiometric ages of the fire clay ton-stein [Pennsylvanian (Upper Caroniferous), Westphaloan, Duckmantian]: a comparison of U–Pb zircon single-crystal ages and $^{40}Ar/^{39}Ar$ sanidine single-crystal plateau ages. Int. J. Coal Geol. 67, 259–266.
Morris, A.W., Bale, A.W., Howland, R.J.M., 1981. Nutrient distribution in an Estuary: Evidence of chemical precipitation of dissolved silicate and phosphate. Estuar. Coast. Shelf Sci. 12, 205–216.
Opluštil, S., Sýkorová, I., 2018. Early Pennsylvanian ombrotrophic mire of the Prokop Coal (Upper Silesian Basin); what does it say about climate? Int. J. Coal Geol. 198, 116–143.
Reimann, C., de Caritat, P., 1998. Chemical Elements in the Environment: Factsheets for the Geochemist and Environmental Scientist. Springer-Verlag, Berlin Heidelberg.
Schmitz, B., Åberg, G., Werdelin, L., Forey, P., Bendix-Almgreen, S.E., 1991. $^{87}Sr/^{86}Sr$, Na, F, Sr, and La in skeletal fish debris as a measure of the paleosalinity of fossil-fish habitats. Geol. Soc. Am. Bull. 103, 786–794.
Schoenbohm, L.M., Burchfiel, B.C., Chen, L.Z., Yin, Y.J., 2006. Miocene to present activity along the Red River fault, China, in the context of continental extrusion, upper-crustal rotation, and lower-crustal flow. Geol. Soc. Am. Bull. 118, 672–688.
Searle, M., 2006. Role of the Red River Shear zone, Yunnan and Vietnam, in the continental extrusion of SE Asia. J. Geol. Soc. 163, 1025–1036.
Shoenbohm, L.M., Burchfiel, B.C., Chen, L.Z., Yin, Y.J., 2005. Exhumation of the Ailao Shan shear zone recorded by Cenozoic sedimentary rocks, Yunnan Province China. Tectonics 24, TC6015. In: doi:10.1029/2005TC001803.
Spears, D., 2017. The role of seawater on the trace element geochemistry of some UK coals and a tribute to Goldschmidt. Minerals 7 (8), 148.
Stach, E., Mackowsky, M.-Th., Teichmüller, M., Taylor, G.H., Chandra, D., Teichmüller, R., 1982. Stach's Textbook of Coal Petrology. Borntraeger, Stuttgart, pp. 1–535.
Stein, M., Starinsky, A., Agnon, A., Katz, A., Raab, M., Spiro, B., Zak, I., 2000. The impact of brine-rock interaction during marine evaporite formation on the isotopic Sr record in the oceans: evidence from Mt. Sedom, Israel. Geochim. Cosmochim. Acta 64, 2039–2053.
Tapponnier, P., Lacassin, R., Leloup, P.H., Scharer, U., Dalai, Z., 1990. The Ailao Shan/Red River metamorphic belt: Tertiary left-lateral shear between Indochina and South China. Nature 343, 431–437.
Tapponnier, P., Xu, Z., Roger, F., Meyer, B., Arnaud, N., Wittlinger, G., Yang, J., 2001. Oblique stepwise rise and growth of the Tibet Plateau. Science 294, 1671–1677.
Tripathy, G.R., Hannah, J.L., Stein, H.J., Geboy, N.J., Ruppert, L.F., 2015. Radiometric dating of marine-influenced coal using Re–Os geochronology. Earth Planet. Sci. Lett. 432, 13–23.
Veizer, J., Compston, W., 1974. $^{87}Sr/^{86}Sr$ composition of sea-water during the Phanerozoic. Geochim. Cosmochim. Acta 40, 905–915.
Veizer, J., Buhl, D., Diener, A., Ebneth, S., Podlaha, O.G., Bruckschen, P., Jasper, T., Korte, C., Schaaf, M., Ala, D., Azmy, K., 1997. Strontium isotope stratigraphy: potential resolution and event correlation. Palaeogeogr. Palaeoclimatol. Palaeoecol. 132, 65–77.
Wang, Z.G., 1995. Atlas of the Sedimentary Facies and Palaeogeography of Yunnan. Yunnan Science and Technology Press. Kunming, China (in Chinese).
Wang, P.L., Lo, C.H., Chung, S.L., Lee, T.Y., Lan, C.Y., Thang, T.V., 2000. Onset timing of left-lateral movement along the Ailao Shan–Red River shear zone: $^{40}Ar/^{39}Ar$ dating constraint from the Nam Dinh area, northeastern Vietnam. J. Asian Earth Sci. 18, 281–292.
Ward, C.R., 2002. Analysis and significance of mineral matter in coal seams. Int. J. Coal Geol. 50, 135–168.
Ward, C.R., 2016. Analysis, origin and significance of mineral matter in coal: An updated review. Int. J. Coal Geol. 165, 1–27.
Xu, L., Bi, X., Hu, R., Zhang, X., Su, W., Qu, W., Hu, Z., Tang, Y., 2012. Relationships between porphyry Cu–Mo mineralization in the Jinshajiang–Red River metallogenic belt and tectonic activity: Constraints from zircon U–Pb and molybdenite Re–Os geochronology. Ore Geol. Rev. 48, 460–473.
Zak, I., 1997. Evolution of the Dead Sea brines. In: Niemi, T.M., Ben-Avraham, Z., Gat, J.R. (Eds.), The Dead Sea, the lake and its setting (Oxford Monographs on Geology and Geophysics, Book 36). Oxford University Press, pp. 133–144.
Zheng, Z.J., Yin, H.W., Zhang, Z., Zheng, M.P., Yang, J.X., 2012. Strontium isotope characteristics and the origin of salt deposits in Mengyejing, Yunnan province. SW China. J. Nanjing Univ. 48, 719–727.